

Experimental study of μ -atomic and μ -molecular processes in pure helium and deuterium-helium mixtures

V. M. Bystritsky,^{1,*} V. F. Boreiko,¹ W. Czapliński,² M. Filipowicz,³ V. V. Gerasimov,¹ O. Huot,⁴ P. E. Knowles,⁴ F. Mulhauser,⁵ V. N. Pavlov,¹ N. P. Popov,² L. A. Schaller,⁴ H. Schneuwly,⁴ V. G. Sandukovsky,¹ V. A. Stolupin,¹ V. P. Volnykh,¹ and J. Woźniak²

¹Joint Institute for Nuclear Research, Dubna 141980, Russia

²AGH University of Science and Technology, Faculty of Physics and Applied Computer Science, PL-30059 Cracow, Poland

³AGH University of Science and Technology, Faculty of Fuels and Energy, PL-30059 Cracow, Poland

⁴Department of Physics, University of Fribourg, CH-1700 Fribourg, Switzerland

⁵University of Illinois at Urbana-Champaign, Urbana, Illinois 61801, USA

(Received 17 December 2003; revised manuscript received 3 December 2004; published 31 March 2005)

We present experimental results of μ -atomic and μ -molecular processes induced by negative muons in pure helium and helium-deuterium mixtures. The experiment was performed at the Paul Scherrer Institute (Switzerland). We measured relative intensities of muonic x-ray K series transitions in $(\mu^{3,4}\text{He})^*$ atoms in pure helium as well as in helium-deuterium mixtures. The $d\mu^3\text{He}$ radiative decay probabilities for two different helium densities in D_2+^3He mixture were also determined. Finally, the q_{1s}^{He} probability for a $d\mu$ atom formed in an excited state to reach the ground state was measured and compared with theoretical calculations using a simple cascade model.

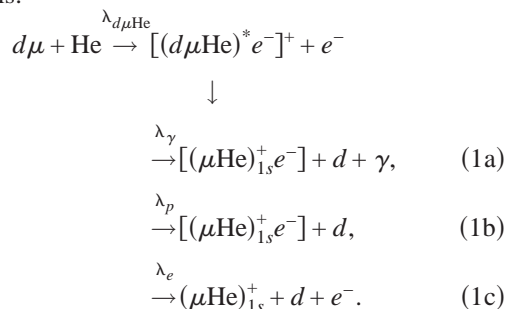
DOI: 10.1103/PhysRevA.71.032723

PACS number(s): 34.70.+e, 36.10.Dr, 39.10.+j, 82.30.Fi

I. INTRODUCTION

The experimental study of atomic and molecular processes induced by negative muons captured in hydrogen and helium provides a test of many-body calculations [1] comprising different methods of atomic, molecular, and nuclear physics. In spite of about 50 years of experimental [2–6] and theoretical [7–11] studies for processes occurring in helium and deuterium, as well as helium-deuterium mixtures, there still exist some open questions. The most important are direct atomic muon capture in H -He mixtures ($H=\text{H}_2, \text{D}_2, \text{T}_2$ and $\text{He}=\text{}^3\text{He}, \text{}^4\text{He}$), initial population of μh ($h=p, d, t$) and μHe excited states for various deexcitation processes of muonic atoms (e.g., Stark mixing, Auger and Coulomb deexcitation processes [12–16]), muon transfer between excited states of μh and μHe [16–20], the probability q_{1s} to reach the μh ground state in a H -He mixture [16,17,20–23], and ground-state muon transfer from μh to helium via the intermediate $2p\sigma$ molecular state $h\mu\text{He}$ [24–28] and the subsequent decay to the unbound $1s\sigma$ state [2,20,22,29,30].

In the case of a deuterium-helium mixture, the $(d\mu\text{He})^*$ molecule, created in $d\mu+\text{He}$ collisions, has three possible decay channels:



Here, λ_γ is the $(d\mu\text{He})^*$ molecular decay channel for the 6.85 keV γ -ray emission, λ_e for the Auger decay, and λ_p for the break-up process. The $(d\mu\text{He})$ molecule is formed, with a rate $\lambda_{d\text{He}}$, in either a $J=0$ or a $J=1$ rotational state (J denotes the total angular momentum of the three particles). The $J=1$ state is mostly populated at slow $d\mu$ -He collisions. The $J=1 \rightarrow J=0$ deexcitation due to inner or external Auger transition is also possible [31–33]. In principle, it competes with the decay processes of Eq. (1a), and can be followed by another decay due to nuclear deuterium-helium fusion from the $J=0$ state [34,35].

In this paper we present experimental results for fundamental characteristics of μ -atomic (MA) and μ -molecular (MM) processes in a D_2+^3He mixture, namely, the muon atomic capture ratio, the q_{1s}^{He} probability, the radiative branching ratio for the radiative decay of the $(d\mu^3\text{He})^*$ molecule (1a), and delayed Lyman series transitions in μHe atoms for two different target densities and at nearly constant helium concentrations. Results for relative intensities of μHe K series transitions in pure ^3He and D_2+^3He for different target densities are also presented.

II. EXPERIMENTAL CONDITIONS

A study of MA and MM processes mentioned above requires the simultaneous use of miscellaneous detectors appropriate for the detection of the muon beam, the muonic x rays of μh and μHe atoms (formed in the target due to direct muon capture by the correspondent nuclei or due to muon transfer from hydrogen to helium), products of nuclear reactions occurring in μh -He complexes, and muon decay electrons. Detection of the latter is necessary not only for yield normalization but also for background reduction. This was realized by requesting that the muon survives atomic and molecular processes. Thus, muon decay electrons were de-

*Electronic address: bystvm@nusun.jinr.ru

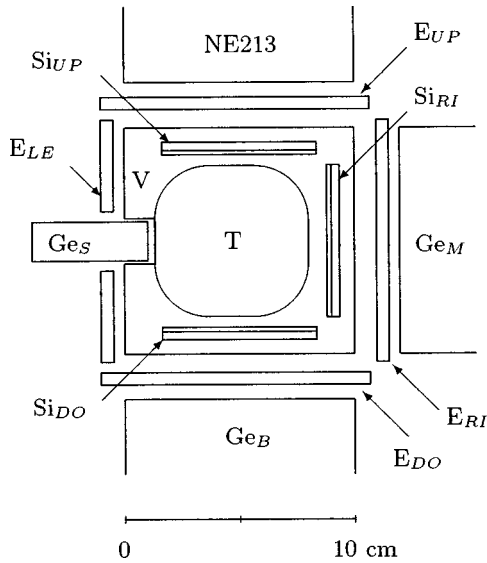
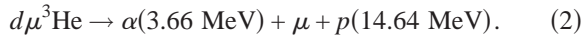


FIG. 1. Scheme of the experimental setup. The view is that of the incoming muon.

ected within a certain time interval after the principal particle detection. For a precise measurement of the characteristics of MA and MM processes the detection system and the associated electronics should have high energy and time resolutions.

The experiment was performed at the Paul Scherrer Institute (PSI) at the μ E4 muon channel. It is described in detail in Refs. [36–38]. A schematic muon view of the setup is given in Fig. 1.

The experimental setup was designed and developed to study nuclear reactions in charge asymmetric muonic molecules such as ($d\mu^3\text{He}$) [34,35,37,39–44]:



Charged reaction products were detected by three silicon telescopes located directly in front of the kapton windows but still within the cooled vacuum environment (Si_{UP} , Si_{RI} , and Si_{DO}). Muon decay electrons were detected by four pairs of plastic scintillators (E_{LE} , E_{UP} , E_{RI} , E_{DO}) placed around the target. The cryogenic target body was made of pure aluminium and had different kapton windows in order to detect in particular the $\sim 34 \text{ MeV}/c$ momentum muon beam, the 6.85 keV γ rays emitted via the radiative decay given in Eq. (1a), and the x-ray Lyman series transitions from the μHe deexcitation ($K\alpha$ at 8.2 keV, $K\beta$ at 9.6 keV, and $K\gamma$ at 10.2 keV). The 0.17 cm^3 germanium detector (Ge_S) used for the γ - and x-ray detection was placed just behind a $55\text{-}\mu\text{m}$ -thick kapton window.

The experiment includes four groups of measurements as depicted in Table I. The first two groups I and II are ^3He and ^4He measurements at different temperatures and pressures. The remaining measurements III and IV were performed with D_2+^3He mixtures at two different densities. The density φ is normalized to the liquid hydrogen density (LHD), $N_0 = 4.25 \times 10^{22} \text{ cm}^{-3}$. Run III was by far the longest run because its original purpose was to measure the fusion rate in

TABLE I. Experimental conditions, such as temperature, pressure, density, and helium concentration. The last column presents the number of muon stops in the gas.

Run	Gas	Temp. [K]	Pressure [atm]	φ [LHD]	c_{He} [%]	N_{stop} [10^6]
I	^3He	32.9			100	
Ia			6.92	0.0363		640.4
Ib			6.85	0.0359		338.1
Ic			6.78	0.0355		375.3
Id			6.43	0.0337		201.7
II	^4He				100	
IIa		20.3	12.55	0.1060		239.4
IIb		19.8	9.69	0.0844		554.1
IIc		20.0	4.52	0.039		32.3
	D_2+^3He	32.8			4.96	
III			5.11	0.0585		4215.6
IV			12.08	0.1680		2615.4

the $d\mu^3\text{He}$ molecule, Eq. (2), and the muon transfer rate $\lambda_{d^3\text{He}}$ from $d\mu$ atoms to ^3He nuclei [37]. The germanium detector energy calibration was carried out during the data taking period using standard sources, namely, ^{60}Co , ^{57}Co , ^{55}Fe , and ^{137}Cs .

III. MEASUREMENT METHOD

The atomic and molecular processes which occur when muons stop in a D_2+^3He mixture are explained in detail in Ref. [38]. Figure 2 schematically presents the essential characteristics of those processes. One distinguishes between prompt and delayed processes. Events occurring within $\pm 0.03 \mu\text{s}$ relative to the muon stop time are called prompt events. The other processes are called delayed ones.

In particular, the prompt processes are the slowing down of muons entering a target to velocities enabling an atomic capture into the excited states of μh or μHe , with a characteristic moderation time $t_{\text{mod}} < 10^{-9} \text{ s}$ for target densities $\varphi > 10^{-3}$ [7,45–48], the formation of excited muonic atoms (μh)*, (μHe)*, $t_{\text{form}} \sim 10^{-11} \text{ s}$ [14], the cascade transitions in (μh)* and (μHe)* muonic atoms $t_{\text{casc}} \sim 10^{-11} \text{ s}$ [49], the muon transfer from excited states of (μh)* to helium (occurring in D_2+^3He mixtures), $t \leq 10^{-10} \text{ s}$ [17,19,20,22].

The delayed processes are the ground-state muon transfer from muonic deuterium to helium [22,28] and the formation of excited ($d\mu^3\text{He}$)* molecules (with the subsequent prompt decay after about 10^{-11} s [29,30]).

A. Pure helium

One of the main characteristics of MA processes occurring in pure helium are absolute and relative intensities of muonic K series x-ray transitions in (μHe)* atoms. Their knowledge provides important information about the excited state initial population of the μHe atoms and the dynamics of

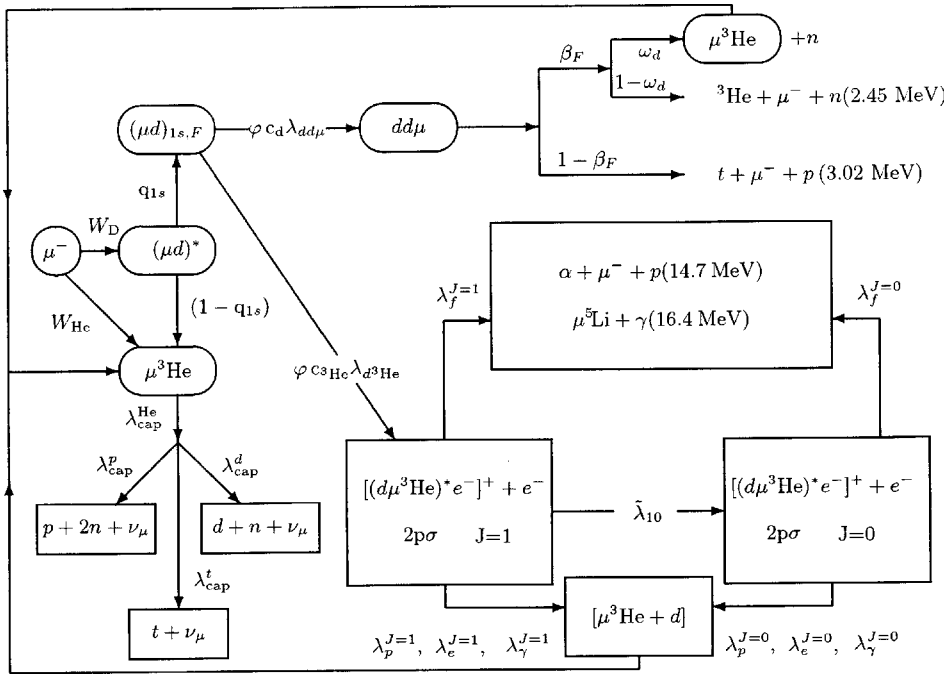


FIG. 2. Scheme of μ -atomic and μ -molecular processes in a $D_2 + {}^3\text{He}$ mixture. Details for all processes and rates are found in Ref. [37].

deexcitation. According to the above given classification of MA processes and the conditions of runs I and II it is clear that only prompt K series transitions from μHe were observed. The chosen prompt time range of ± 30 ns is a consequence of the detector and its related electronic time resolution. The relative intensities I_x^{He} of the Kx lines ($x \equiv \alpha, \beta, \gamma$) are

$$I_x^{\text{He}} = \frac{Y_x^{\text{He}}}{Y_{\text{tot}}^{\text{He}}} \quad \text{with} \quad \sum_{x=\alpha,\beta,\gamma} I_x^{\text{He}} = 1, \quad (3)$$

where $Y_\alpha^{\text{He}}, Y_\beta^{\text{He}}, Y_\gamma^{\text{He}}$ are the yields of μHe Kx lines with energies 8.17, 9.68, and 10.2 keV, respectively. These yields are determined as follows:

$$Y_x^{\text{He}} = \frac{N_x^{\text{He}}}{\eta_x \varepsilon_x}, \quad Y_{\text{tot}}^{\text{He}} = \sum_{x=\alpha,\beta,\gamma} Y_x^{\text{He}} \quad (4)$$

with $Y_{\text{tot}}^{\text{He}}$ being the total yield of all Kx lines. The quantities N_x^{He} are the numbers of prompt events corresponding to the μHe Kx lines, the factors η_x describe the attenuation of these lines when passing through the gas mixture and kapton windows toward the Ge_S detector, and ε_x are the corresponding detection efficiencies. The I_γ^{He} intensity is the cumulative photon yield of the Lyman series $n \geq 4$.

In fact, only detection efficiency ratios ($\varepsilon_{x\alpha} = \varepsilon_x / \varepsilon_\alpha$) are required for the determination of the relative intensities. Therefore Eq. (3) can be rewritten as

$$I_x^{\text{He}} = \frac{N_x^{\text{He}}}{N_{\text{tot}}^{\text{He}} \eta_x \varepsilon_{x\alpha}}, \quad (5)$$

with

$$N_{\text{tot}}^{\text{He}} = \sum_{x=\alpha,\beta,\gamma} \frac{N_x^{\text{He}}}{\eta_x \varepsilon_{x\alpha}} \quad (6)$$

being the total yield normalized to the detection efficiency ε_α . This fact significantly increases the accuracy of I_x^{He} measured in the experiment. The corresponding errors were mainly due to insufficient knowledge of the respective attenuation factors η_x . However, on the basis of the attenuation coefficient values compiled in Ref. [50], we estimated that these factors differ only slightly because the differences between the energies of Kx lines [$\Delta E_{\beta-\alpha} = E(K\beta) - E(K\alpha) = 1.51$ keV, $\Delta E_{\gamma-\alpha} = E(K\gamma) - E(K\alpha) = 2.03$ keV] are relatively small, and the thickness of all the layers placed before the Ge_S detector are small too. In recent experiments, similar assumptions were also used (see Refs. [20,28]).

The detection efficiencies ε_x are determined using Eqs. (3) and (4) via

$$\varepsilon_x = \frac{N_x^{\text{He}}}{N_{\text{stop}}^{\text{He}} I_x^{\text{He}}}, \quad (7)$$

where $N_{\text{stop}}^{\text{He}}$ is the number of muons stopping in helium, given in Table I. For an accurate determination of the attenuation of the K series transitions we performed Monte Carlo (MC) calculations taking into account the experimental geometry and all material layers placed between the x-ray emission and the germanium detector. The attenuation factor η_x for each Kx line includes the x-ray attenuation when passing through the gas target and the chamber kapton window, and through the germanium detector Be window (see also Ref. [51]). We obtained $\eta_\alpha = 0.844$, $\eta_\beta = 0.915$, and $\eta_\gamma = 0.925$.

A significant reduction of the germanium detector background was achieved by using delayed coincidences between x-rays and electrons. This method is called the “del- e ” crite-

tion. Ground state muonic helium atoms disappear mainly by muon decay,

$$\mu^- \rightarrow e^- + \nu_\mu + \bar{\nu}_e, \quad (8)$$

and by nuclear muon capture (with proton, deuteron, or triton emission [38,52,53]). The average disappearance rate is

$$\lambda_{\text{He}} = \lambda_0 + \lambda_{\text{cap}}^{\text{He}} \approx 0.457 \times 10^6 \text{ s}^{-1}, \quad (9)$$

where $\lambda_0 = 0.455 \times 10^6 \text{ s}^{-1}$ and $\lambda_{\text{cap}}^{\text{He}} = 2216(70) \text{ s}^{-1}$ [52]. Thus, delayed electrons were measured during a time interval corresponding to two μHe atom lifetimes ($\tau_{\text{He}} = 2.19 \mu\text{s}$ [54]).

The relative intensities of the Kx lines I_{x-e}^{He} , detected in coincidence with muon decay electrons, are given by

$$I_{x-e}^{\text{He}} = \frac{1}{\varepsilon_e f_t} \frac{N_{x-e}^{\text{He}}}{N_{\text{tot},e}^{\text{He}} \eta_x \varepsilon_{x\alpha}} \quad (10)$$

with

$$N_{\text{tot},e}^{\text{He}} = \frac{1}{\varepsilon_e f_t} \sum_{x=\alpha,\beta,\gamma} \frac{N_{x-e}^{\text{He}}}{\eta_x \varepsilon_{x\alpha}}, \quad (11)$$

where N_{x-e}^{He} are the number of events in pure helium detected by the germanium detector in coincidence with muon decay electrons within a fixed time interval $\Delta t = t_e - t_\gamma$, with t_γ and t_e the time of a detected events in the germanium and decay electron counters, respectively. Both times are measured relative to the muon stop time $t=0$. ε_e is the detection efficiency of muon decay electrons and the time factor

$$f_t = 1 - e^{-\lambda_{\text{He}} \Delta t} \quad (12)$$

is the probability that a muon decays in the ground state of μHe during the time interval Δt .

It should be noted, that the coefficient $\varepsilon_e f_t$ is not required as an absolute number for the determination of the intensities I_{x-e}^{He} as it enters the numerator and denominator of Eq. (10) in the same manner. However, it is needed for the $\text{D}_2 + {}^3\text{He}$ analysis. The quantity $\varepsilon_e f_t$ is determined by comparing Eqs. (5) and (10) yielding

$$\varepsilon_e f_t = \frac{N_{x-e}^{\text{He}}}{N_x^{\text{He}}}. \quad (13)$$

Another interesting problem is the study of μHe atoms in excited metastable $2s$ states. One can expect, according to Refs. [55–58], that the $(\mu\text{He})_{2s}$ atom population varies between 5 and 7% under our experimental conditions for runs I and II. The two possible channels for $2s \rightarrow 1s$ deexcitation are two-photon transition with a rate $\lambda_{2\gamma} \sim 1.06 \times 10^5 \text{ s}^{-1}$ [59,60] and Stark $2s \rightarrow 2p \rightarrow 1s$ deexcitation [55–57] induced by collisions of $(\mu\text{He})_{2s}$ atoms with the surrounding atoms or molecules. The corresponding rate for the experimental conditions of runs I and II is $\lambda \sim 2.2 \times 10^7 \text{ s}^{-1}$. If the time of Stark $2s \rightarrow 2p \rightarrow 1s$ deexcitation is shorter than the resolution time of the germanium detector, the corresponding $K\alpha$ transition would be experimentally classified as a prompt event. Otherwise, it would be possible to extract an upper bound for the rates of Stark induced transitions.

B. $\text{D}_2 + {}^3\text{He}$ mixtures

In a $\text{D}_2 + {}^3\text{He}$ mixture one observes Kx lines arising from the deexcitation of μHe atoms formed not only due to direct muon capture by helium nuclei (as in pure helium) but also due to muon transfer from muonic deuterium to helium. Because the $d\mu$ atom deexcitation time is of the order 10^{-11} s (under our experimental conditions) the corresponding emission of K series transitions occurs practically immediately after a muon stop in the mixture and can be classified as a prompt event. Muons are captured by D_2 and ${}^3\text{He}$ according to the capture law [2]. The corresponding relative probability has the following form [21,61–64]:

$$W_{\text{D}} = \frac{1}{1 + Ac}, \quad W_{\text{He}} = \frac{Ac}{1 + Ac}, \quad (14)$$

where $c = c_{\text{He}}/c_{\text{D}}$ is the ratio of atomic concentrations of helium to deuterium, c_{He} and c_{D} are the relative atomic helium and deuterium concentrations in the $\text{D}_2 + {}^3\text{He}$ mixture, A is the muon atomic capture ratio

$$A = \frac{A_{\text{He}}}{A_{\text{D}}}, \quad (15)$$

with A_{He} and A_{D} the muon capture probability per one helium and deuterium atom, respectively. We used the averaged value $A = (1.7 \pm 0.2)$ [2,21,61–67] for the analysis of our measurements. Information about the probability q_{1s}^{He} , that an excited $(d\mu)^*$ atom reaches its ground state when the muon also has the possibility of transferring directly from an excited state to a heavier nucleus (in our case helium) is of unquestionable importance for understanding kinetics in muon catalyzed fusion (μCF). A method for determining the characteristics of MA processes in the $\text{D}_2 + {}^3\text{He}$ mixture is presented in the following subsections.

1. The q_{1s}^{He} probability

Prompt Lyman series transitions in μHe atoms are observed in a $\text{D}_2 + {}^3\text{He}$ mixture. As mentioned previously, they originate from direct muon capture by deexcitation of $(\mu\text{He})^*$ atoms or by muon transfer from excited muonic deuterium to helium. However, the relative intensities of K series transitions measured in a $\text{D}_2 + {}^3\text{He}$ mixture differ from the ones in pure helium because effective reaction rates of μHe deexcitation processes depend on the target conditions. q_{1s}^{He} represents the $(d\mu)^*$ atom probability to reach the ground state in a $\text{D}_2 + {}^3\text{He}$ mixture and is defined as

$$q_{1s}^{\text{He}} = \frac{n_{d\mu}^{1s}}{n_{d\mu}^*}, \quad (16)$$

where $n_{d\mu}^*$ is the number of $d\mu$ atoms created in the excited state due to direct muon capture in deuterium atoms and $n_{d\mu}^{1s}$ is the number of the $d\mu$ atoms which reach the ground state during the cascade. The number of $d\mu$ atoms created in the excited state can be written as

$$n_{d\mu}^* = N_{\text{stop}}^{\text{D/He}} W_{\text{D}}, \quad (17)$$

where $N_{\text{stop}}^{\text{D/He}}$ represents the number of muon stops in the $\text{D}_2 + {}^3\text{He}$ gas mixture.

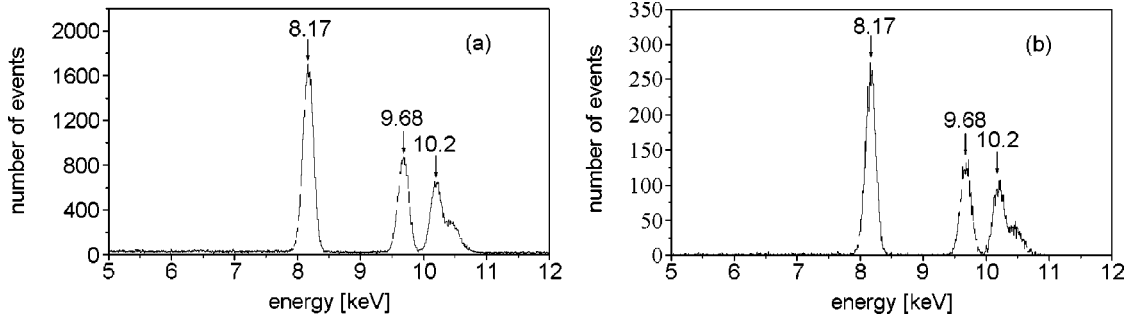


FIG. 3. Energy distribution of prompt events in run I without (a) and with coincidences with muon decay electrons (b).

Since our setup is not able to measure $n_{d\mu}^{1s}$, we used another method to determine q_{1s}^{He} . The number of μHe atoms formed in excited states due to muon transfer from $(d\mu)^*$ to helium, $(d\mu)^* + \text{He} \rightarrow (\text{He}\mu)^* + d$, is $n_{\text{He}\mu^*}^{\text{transf}}$ and corresponds to

$$n_{\text{He}\mu^*}^{\text{transf}} = n_{d\mu}^* - n_{d\mu}^{1s}. \quad (18)$$

The total number of μHe atoms created in the excited states and emitting prompt Kx lines is given by the yield

$$Y_{\text{tot}}^{\text{D/He}} = \sum_{x=\alpha,\beta,\gamma} \frac{N_x^{\text{D/He}}}{\eta_x \varepsilon_x}. \quad (19)$$

On the other hand, $n_{\text{He}\mu^*}^{\text{dir}}$ is the number of μHe atoms formed in the excited states in a $\text{D}_2 + {}^3\text{He}$ mixture due to direct muon capture by helium atoms

$$n_{\text{He}\mu^*}^{\text{dir}} = Y_{\text{tot}}^{\text{D/He}} - n_{\text{He}\mu^*}^{\text{transf}} = N_{\text{stop}}^{\text{D/He}} W_{\text{He}}. \quad (20)$$

Isolating $n_{d\mu}^{1s}$ in Eq. (18) and using Eqs. (17) and (20), we obtain the q_{1s}^{He} probability as

$$q_{1s}^{\text{He}} = (1 + A c_{\text{He}}) \left[1 - \frac{Y_{\text{tot}}^{\text{D/He}}}{N_{\text{stop}}^{\text{D/He}}} \right]. \quad (21)$$

In the case of detecting events by the germanium detector in coincidence with muon decay electrons, the total yield $Y_{\text{tot}}^{\text{D/He}}$ in Eq. (21) has to be replaced by

$$Y_{\text{tot,e}}^{\text{D/He}} = \frac{1}{\varepsilon_e f} \sum_{x=\alpha,\beta,\gamma} \frac{N_{x-e}^{\text{D/He}}}{\eta_x \varepsilon_x}. \quad (22)$$

2. Radiative molecular peak

The delayed muonic x-rays are generated by two different mechanisms initiated by $d\mu$ atoms in their ground state. The first mechanism described in this section is simply molecular muon transfer, specifically Eq. (1a) accompanied by a 6.85 keV γ ray. Experimental molecular muon transfer from muonic deuterium to helium $\lambda_{d^3\text{He}}$ is presented in detail in many papers, in particular in Refs. [31,38] together with the corresponding reaction rates. The radiative decay rate of the $d\mu^3\text{He}$ complex Eq. (1a) can be measured as follows.

The time distribution of the γ rays (relative to the muon stop time) decreases experimentally with the disappearance rate of the muonic deuterium ground state $\lambda_{d\mu}$,

$$\frac{dN_{6.85}}{dt} = A_{d\mu} e^{-\lambda_{d\mu} t}, \quad (23)$$

with $A_{d\mu}$ the amplitude and

$$\lambda_{d\mu} = \lambda_0 + \lambda_{d^3\text{He}} \varphi c_{\text{He}} + \tilde{\lambda}_{dd\mu} \varphi c_{\text{D}} [1 - W_{\text{D}} q_{1s}^{\text{He}} (1 - \beta \omega_d)]. \quad (24)$$

$\lambda_{d^3\text{He}}$ is the molecular formation rate for the $d\mu^3\text{He}$ molecule and $\lambda_0 = 0.455 \times 10^6 \text{ s}^{-1}$ is the free muon decay rate. $\tilde{\lambda}_{dd\mu}$ is the effective $dd\mu$ molecule formation rate, β the relative probability of nuclear fusion in $dd\mu$ with neutron production in the final channel, and ω_d is the muon sticking probability to helium produced in nuclear $d-d$ fusion (see Ref. [38]).

The probability of the radiative decay of the $\text{D}\mu^3\text{He}$ system (corresponding to the $2p\sigma \rightarrow 1s\sigma$ transition) is defined by

$$\kappa_{d\mu\text{He}} = \frac{\lambda_\gamma}{\lambda_p + \lambda_\gamma + \lambda_e}, \quad (25)$$

where λ_γ , λ_p , and λ_e are the reaction rates for the $d\mu^3\text{He}$ molecular decay according to the three channels (1a)–(1c), respectively, also shown in Fig. 2. The formation of the $d\mu^3\text{He}$ molecule practically coincides with the subsequent γ -ray emission because of the very short average lifetime of $d\mu^3\text{He}$ molecule ($\sim 10^{-11} \text{ s}$ [2,20,22,28,29]).

In the present experiment only the radiative decay channel is detected. The corresponding $\kappa_{d\mu\text{He}}$ probability is determined by the ratio

$$\kappa_{d\mu\text{He}} = \frac{N_{\gamma}^{d\mu^3\text{He}}}{N_{\text{tot}}^{d\mu^3\text{He}}}, \quad (26)$$

where $N_{\text{tot}}^{d\mu^3\text{He}}$ and $N_{\gamma}^{d\mu^3\text{He}}$ are the total number of $d\mu^3\text{He}$ molecules formed in the mixture and the number of molecules subsequently decaying via the radiative channel. The latter quantity may be expressed as

$$N_{\gamma}^{d\mu^3\text{He}} = \frac{N_{6.85}}{\varepsilon_{6.85} F_t \eta_{6.85}}, \quad (27)$$

where $N_{6.85}$ is the number of 6.85 keV γ rays detected during the time Δt_γ elapsed after a muon stop and $\varepsilon_{6.85}$ is the corresponding detection efficiency. The factor F_t

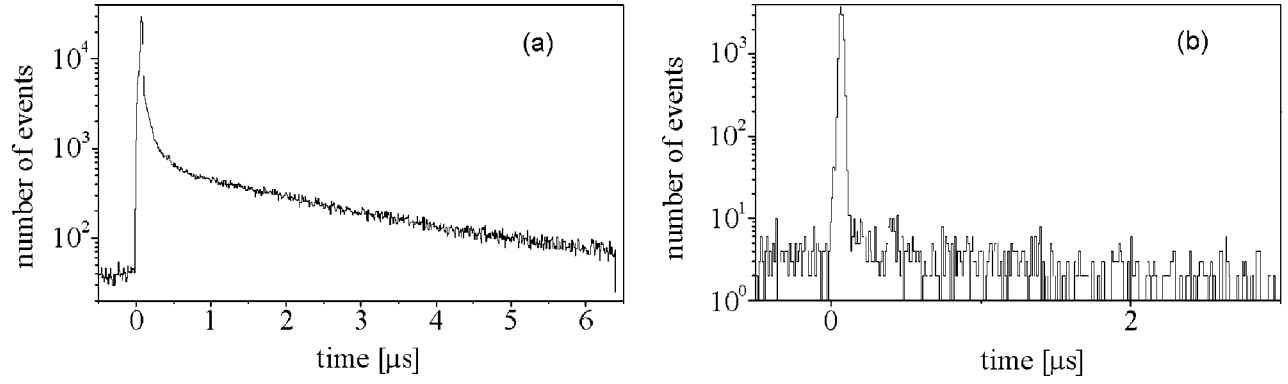


FIG. 4. Time distribution in run I without (a) and with coincidences with muon decay electrons (b).

$$F_t = e^{-\lambda_{d\mu}t}(1 - e^{-\lambda_{d\mu}\Delta t_{\gamma}}) \quad (28)$$

is the γ -ray detection time factor and $\eta_{6.85}$ is the 6.85 keV γ -ray attenuation factor. For the γ rays detected with the del- e criterion, a corresponding $N_{\gamma}^{d\mu^3\text{He}}$ value is obtained using Eq. (27) divided by the $\varepsilon_e f_t$ coefficients.

A comparison of the $N_{\gamma}^{d\mu^3\text{He}}$ value measured with and without the del- e criterion provides also a test for the validity of our coefficients ε_e , f_t , and $N_{6.85}$. The detection efficiency $\varepsilon_{6.85}$ was determined by MC simulations including feasible space distributions of muon stops in the target volume and experimental detection efficiencies of Kx lines for the pure ^3He runs.

The total number of the $d\mu^3\text{He}$ molecules formed in a D_2+He mixture is determined by analyzing the 6.85 keV γ -ray time distribution. It is expressed as

$$N_{\text{tot}}^{d\mu^3\text{He}} = \frac{\lambda_{d^3\text{He}} \varphi C_{\text{He}}}{\lambda_{d\mu}} n_{d\mu}^{1s}, \quad (29)$$

where $n_{d\mu}^{1s}$ is the number of $d\mu$ atoms formed via direct muon capture and reaching the ground state after deexcitation. By measuring the exponential time distribution (23) and using the known quantities λ_0 , $\tilde{\lambda}_{dd\mu}$, W_D , ω_d , q_{1s}^{He} , and β [68–70] one can determine the molecular formation rate $\lambda_{d^3\text{He}}$ from Eq. (24). The determination of $N_{d\mu^3\text{He}}^{\text{tot}}$ from Eq. (29) requires in addition the knowledge of $n_{d\mu}^{1s}$, determined from Eqs. (16) and (17). By substituting $N_{\gamma}^{d\mu^3\text{He}}$ and $N_{\text{tot}}^{d\mu^3\text{He}}$ into Eq. (26) one finally obtains the $\kappa_{d\mu\text{He}}$ probability.

3. Delayed K series transitions from muonic helium

As previously said, the delayed muonic x rays are generated by two different mechanisms initiated from the ground state $d\mu$ atoms. The second one discussed here starts with the $dd\mu$ formation, due to collision of a $(d\mu)_{1s}$ atom with a D_2 molecule, subsequently followed by nuclear $d-d$ fusion. Muons freed after fusion form excited muonic helium atoms due to direct muon capture by helium or due to muon capture by deuterium and subsequent muon transfer to helium. Then the delayed x rays of muonic helium K series transitions are observed.

The time distribution is also determined by $\lambda_{d\mu}$. In addition, the relative intensities $I_{x,\text{del}}$ (or $I_{x-e,\text{del}}$) of the delayed K series transitions are assumed to be the same as those of the prompt radiation of Kx lines. It is worthwhile to note that the measurement of the corresponding absolute intensities enabled us to determine the third component of $\lambda_{d\mu}$ in Eq. (24) and, consequently, to extract the effective formation rate of the $dd\mu$ molecule in the D_2+^3He mixture using the coefficients W_D , q_{1s}^{He} (also obtained in this paper) and average values for β and ω_d (taken from Refs. [68–70]).

IV. ANALYSIS

A. Relative intensities of K series transitions

To obtain the relative intensities of muonic x-ray K series transitions of $\mu^3\text{He}$ and $\mu^4\text{He}$ atoms in helium targets, we analyzed the corresponding energy and time distributions detected by the germanium detector in runs I and II. Figures 3 and 4 present the energy and time distributions obtained in runs I with and without muon decay electrons coincidences.

 TABLE II. Prompt x-ray yields of $\mu^{3,4}\text{He}$ K series transitions measured in runs with pure ^3He and ^4He .

Range [keV] Runs	$K\alpha$ [7.83–8.53]		$K\beta$ [9.43–9.96]		$K\gamma$ [9.98–10.6]		Yield [10 ⁸]	Yield [10 ⁸]	Yield [10 ⁸]
	N_{α}^{He}	$N_{\alpha-e}^{\text{He}}$	N_{β}^{He}	$N_{\beta-e}^{\text{He}}$	N_{γ}^{He}	$N_{\gamma-e}^{\text{He}}$			
I (^3He)	34 319(190)	4785(70)	17 835(139)	2551(52)	20 045(150)	2834(54)	7.536(90)	3.795(53)	4.231(62)
IIa (^4He)	7295(87)	985(32)	4919(72)	688(26)	2616(55)	408(20)	0.897(14)	0.585(10)	0.309(8)
IIb (^4He)	11 587(111)	1593(40)	7547(91)	1009(32)	4627(76)	613(25)	1.766(25)	1.126(18)	0.677(13)
IIc (^4He)	1303(38)	174(14)	709(29)	91(10)	846(33)	123(12)	0.287(9)	0.151(6)	0.178(7)

TABLE III. Relative intensities of prompt x rays of $\mu^{3,4}\text{He}$ K series transitions measured in runs with pure helium. For each run, results from both the full statistics and the del- e condition are given.

	I_{α}^{He} [%]	$I_{\alpha-e}^{\text{He}}$ [%]	I_{β}^{He} [%]	$I_{\beta-e}^{\text{He}}$ [%]	I_{γ}^{He} [%]	$I_{\gamma-e}^{\text{He}}$ [%]
I (^3He)	48.4(4)	47.8(5)	24.4(3)	24.8(4)	27.2(3)	27.4(5)
IIa (^4He)	50.0(5)	47.3(11)	32.7(5)	33.1(10)	17.3(4)	19.6(9)
IIb (^4He)	49.5(5)	49.5(9)	31.5(4)	31.4(8)	19.0(3)	19.1(7)
IIc (^4He)	46.6(10)	44.8(27)	24.5(9)	23.5(23)	28.9(10)	31.7(25)
Augsburger <i>et al.</i> [20] (^4He)	46.9(45)		27.9(28)		25.2(19)	
Tresch <i>et al.</i> [22] ^a	47.0(2)		20.3(10)		32.7(16)	

^aFor ^3He ($\varphi=0.026$) and for ^4He ($\varphi=0.0395$).

As seen, the del- e criterion significantly suppressed the background level and improved the signal-to-background ratio. As already mentioned before, events detected within a time interval $t_{\gamma}=[(-0.03)-(0.03)] \mu\text{s}$ relative to muon stops were classified as prompt ones. The prompt Kx lines events N_x^{He} , N_{x-e}^{He} were determined by fitting the experimental amplitude distributions by a Gaussian distribution

$$\frac{dN_x^{\text{He}}}{dE_x} = A_x \exp\left[-\frac{(E_x - \bar{E}_x)^2}{2\sigma_x^2}\right] + SE_x + O, \quad (30)$$

where \bar{E}_x is the mean value of the corresponding Kx line energy, σ_x the standard deviation for the Kx line and A_x the normalization constant. The germanium detector background is taken into account by a straight line, with S and O being the constants. Results obtained in measurements I and II are presented in Tables II and III. The agreement with other experiments [20,22] as well as with the theoretical prediction [9] is very good. Statistical errors are quoted in parentheses throughout the whole text.

The analysis performed for both mixtures is similar. The prompt intensities are measured within the same time interval as for the pure helium runs, both with and without the delayed electron coincidence condition. The results, given in Table IV, depend on the pressure of the D_2+^3He mixture. For comparison, results of Augsburger *et al.* [20] taken at a similar pressure as in run III, are also shown in the table. The differences in relative intensity between pure helium and the deuterium-helium mixtures are essentially due to excited state transfer. Additionally, such an analysis allows us to determine the Kx transition energy differences between the two

TABLE IV. Relative intensities, in percent, of prompt x rays of $\mu^3\text{He}$ K series transitions measured in runs III and IV. "Full" stands for full statistics, whereas del- e represents the delayed electron criterion. The last column shows the results of Augsburger *et al.* [20].

Runs Transitions	III		IV		Augsburger <i>et al.</i> [20]
	full	del- e	full	del- e	
$I_{\alpha}^{\text{D/He}}$	66.4(4)	65.7(7)	72.0(3)	72.9(6)	68.6(51)
$I_{\beta}^{\text{D/He}}$	26.6(3)	26.5(6)	24.5(2)	24.1(6)	24.5(19)
$I_{\gamma}^{\text{D/He}}$	7.0(3)	7.8(4)	3.5(1)	3.0(3)	6.9(6)

helium isotopes. The $\Delta E(^4\text{He}-^3\text{He})$ energy difference is given in Table V for the different transitions. A theoretical prediction for the $K\alpha$ transition [71] is slightly lower than our measured value.

B. q_{1s}^{He} probability

One of the main aim of runs III and IV was a measurement of the q_{1s}^{He} probability. In order to determine this quantity it was necessary to know [according to Eqs. (16)–(21)] the muon atomic capture ratio A , the prompt K series transition yields of $\mu^3\text{He}$ atoms in pure ^3He and in D_2+^3He mixtures N_x^{He} and $N_x^{\text{D/He}}$ and the number of muon stops in pure ^3He and in D_2+^3He mixtures N_{stop} . Significant background reduction was achieved by using the del- e criterion. The results are presented in Table VI. Note the excellent agreement between full statistics and del- e analysis.

Figure 5 shows the energy dependence of the theoretical q_{1s}^{He} values vs $d\mu+^3\text{He}$ collision energy calculated for runs III and IV in the framework of the simple $(d\mu)^*$ cascade model [16,17,72] and their comparison with experiment. The model assumes that the kinetic energy of $(d\mu)^*$ atoms remains unchanged during deexcitation. The q_{1s}^{He} value is determined from deexcitation and muon transfer to helium. The complicated interplay between these two processes is described by a system of linear first-order differential equations for level populations $N_n(t)$, with $n \leq 12$. The q_{1s}^{He} is defined as

$$q_{1s} = N_{1s}(t \rightarrow \infty). \quad (31)$$

The deexcitation scheme is taken from Ref. [17] and the corresponding reaction rates are collected in Refs. [16,17].

TABLE V. Kx transition energy differences between the two helium isotopes. The last column gives a theoretical prediction for the $K\alpha$ transition.

Transitions	$\Delta E(^4\text{He}-^3\text{He})$ [eV]		
	Our work	Tresch <i>et al.</i> [22]	Rinker [71]
$K\alpha$	77.8 ± 0.9	75.0 ± 1.0	74.2
$K\beta$	92.9 ± 1.1		
$K\gamma$	103.4 ± 3.4		

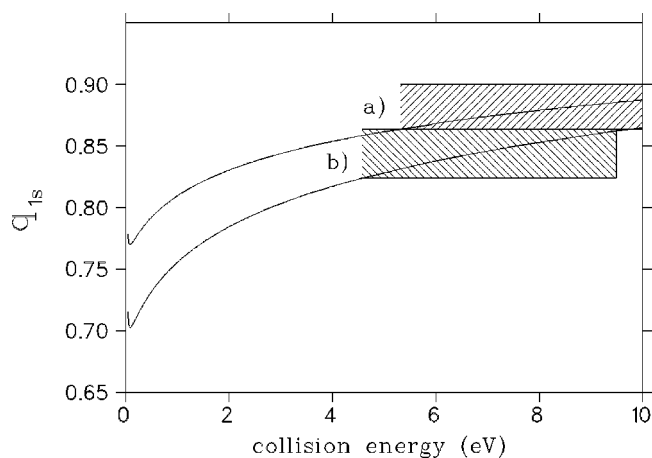


FIG. 5. Energy dependence of q_{1s}^{He} in the $\text{D}_2 + {}^3\text{He}$ mixture calculated for runs III (curve a) and IV (curve b). Experimental values of q_{1s}^{He} measured in the present work [$q_{1s}^{\text{He}} = (0.882 \pm 0.018)$ and $q_{1s}^{\text{He}} = (0.844 \pm 0.020)$] are represented by hatched boxes.

As seen from Fig. 5, the experimental values of q_{1s}^{He} coincide with the theoretical ones for an average $d\mu$ -He collision energy of around 8 eV. Note the pronounced difference between the experimental values of q_{1s}^{He} and the theoretical ones corresponding to fully thermalized $d\mu$ atoms. However, more refined theoretical calculations of q_{1s}^{He} based on Monte Carlo simulations of acceleration of $d\mu$ atoms due to deexcitation processes and muon transfer to helium as well as thermalisation due to elastic collisions are required to arrive at definite conclusions. It should also be noted that experimental results presented in this paper agree with earlier ones (see Ref. [73]). On the other hand, an analogous comparison with results presented in Refs. [20–22,62] is not possible due to significantly different helium concentrations and densities.

C. Radiative branching ratio $\kappa_{d\mu\text{He}}$

The experimental method to determine the $d\mu^3\text{He}$ radiative decay branching ratio $\kappa_{d\mu\text{He}}$ is described in Sec. III B 2. Energy and time distributions of prompt and delayed events detected in runs III and IV with muon decay electrons coincidences are presented in Figs. 6–8.

To determine the $\lambda_{d\mu}$ and $\lambda_d^3\text{He}$ rates [see Eq. (24)] the γ -ray time distributions were fitted within an energy range 5.74–7.50 keV using the expression

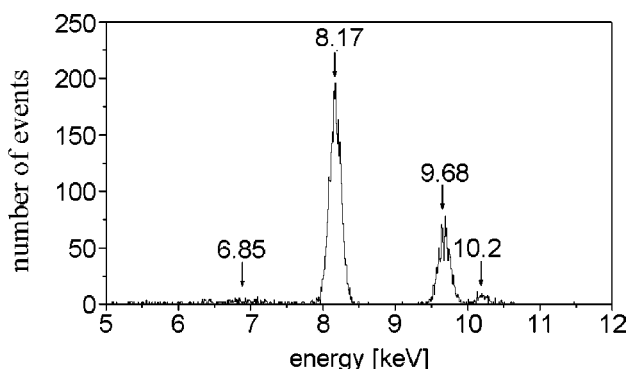
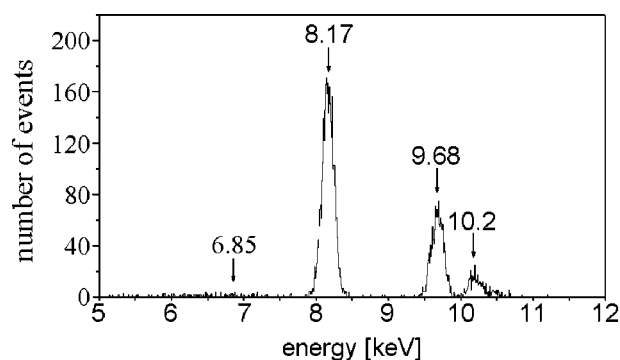


FIG. 6. Energy spectra of the prompt events in runs III (left) and IV (right).

TABLE VI. Experimental values of q_{1s}^{He} obtained from the $\text{D}_2 + {}^3\text{He}$ experiments. Full stands for the full statistics, whereas del-e represent the delayed electron criterion.

Runs	Statistics	$\sum_{x=\alpha,\beta,\gamma} N_x^{\text{D/He}}$	$Y_{\text{tot}}^{\text{D/He}}$ [10^8]	q_{1s}^{He}
III	full	35 376(270)	7.70(15)	0.882(18)
	del-e	4968(72)	7.60(29)	0.885(21)
IV	full	37 402(205)	5.71(11)	0.844(20)
	del-e	5161(75)	5.85(23)	0.838(23)

$$\frac{dN_{6.85}}{dt} = A_{d\mu}^{\gamma} e^{-\lambda_{d\mu} t} + A_{\text{Au}}^{\gamma} e^{-\lambda_{\text{Au}} t} + A_{\text{Al}}^{\gamma} e^{-\lambda_{\text{Al}} t} + D^{\gamma} e^{-\lambda_0 t} + F^{\gamma}, \quad (32)$$

where $A_{d\mu}^{\gamma}$, A_{Au}^{γ} , and A_{Al}^{γ} are the normalization constants of the different target elements. D^{γ} and F^{γ} are the constants describing the germanium background.

The results of runs III and IV for the ground state disappearance rate of muonic deuterium and the molecular formation rate $\lambda_d^3\text{He}$, using Eq. (24), are shown in Table VII. The averaged value $\lambda_d^3\text{He} = 242(20) \mu\text{s}^{-1}$, where the errors include statistical as well as systematic errors is consistent with the measurement of Maev *et al.* [74], but in disagreement with the work of Gartner *et al.* [28].

According to Eq. (26) the determination of the branching ratio $\kappa_{d\mu\text{He}}$ requires the knowledge of both the total number of $d\mu^3\text{He}$ molecules formed in a mixture and the number of $d\mu^3\text{He}$'s decaying via the radiative channel, Eq. (1a). The corresponding numbers $N_{\text{tot}}^{d\mu^3\text{He}}$ and $N_{\gamma}^{d\mu^3\text{He}}$ were determined using Eqs. (27) and (29). The γ rays were measured during a time t_{γ} and the del-e time interval was $t_e - t_{\gamma}$. The detection efficiency $\varepsilon_{6.85}$ was determined using detection efficiencies of $\mu^3\text{He}$ atom K series transitions in runs I and II by a MC simulation. This MC calculation took into account the $\eta_{6.85}$ attenuation of γ rays passing through all layers between the germanium detector and the gas. The time factors f_i for the electrons and F_i for the γ rays are slightly different for both runs, $f_i = 0.84$ and $F_i = 0.94$ for run III and $f_i = 0.86$ and $F_i = 0.99$ for run IV. All results are presented in Table VIII.

The $\kappa_{d\mu\text{He}}$ values obtained in the present experiment for two different $\text{D}_2 + {}^3\text{He}$ densities differ somewhat from the

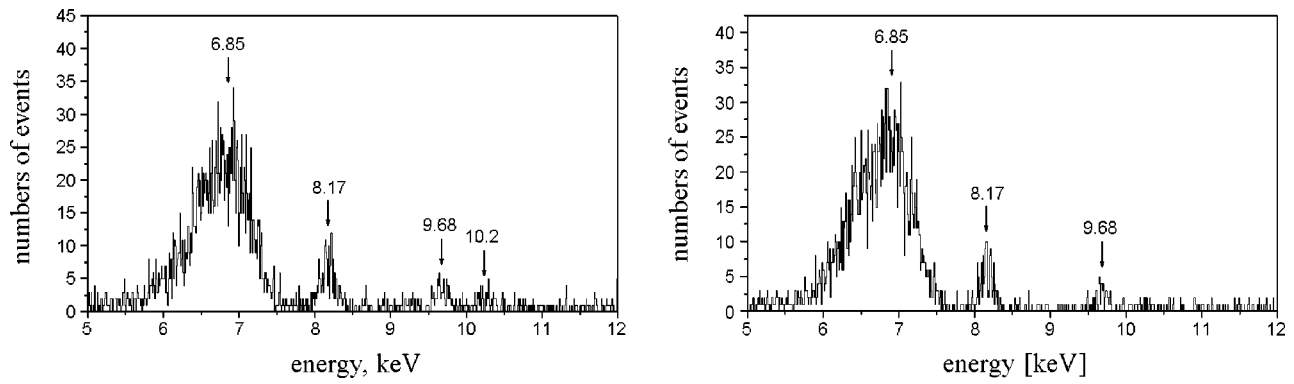
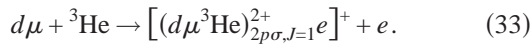


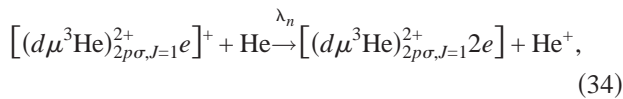
FIG. 7. Energy spectra of the delayed events in runs III (left) and IV (right).

experimental result of Ref. [20], i.e., $\kappa_{d\mu\text{He}} = (0.301 \pm 0.061)$ performed under slightly different experimental conditions ($\varphi = 0.0697$, $c_{\text{He}} = 0.0913$). Our results differ slightly from the calculated $\kappa_{d\mu\text{He}}$ value in Ref. [30] for a total angular momentum $J=0$ of the $d\mu^3\text{He}$ complex. However, they are in a good agreement with the calculations of Refs. [29,75] for a total angular momentum $J=1$.

A close comparison of the existing theoretical results for $\kappa_{d\mu\text{He}}$, [27,29,30,75–77], with the experimental results obtained in the present paper and in Ref. [20] may throw some light on the mechanism of rotational $J=1 \rightarrow J=0$ transitions of $d\mu^3\text{He}$ molecules in the $2p\sigma$ state, labeled $\tilde{\lambda}_{10}$ in Fig. 2. Specifically, two different mechanism of the $J=1 \rightarrow J=0$ transition were proposed in Refs. [31–34]. Both mechanisms start with an Auger transition in a $d\mu + ^3\text{He}$ collision



The first mechanism [31–33] consists of a two stage process, namely, the formation of a neutral complex in the collision



followed by a subsequent deexcitation due to external Auger effect

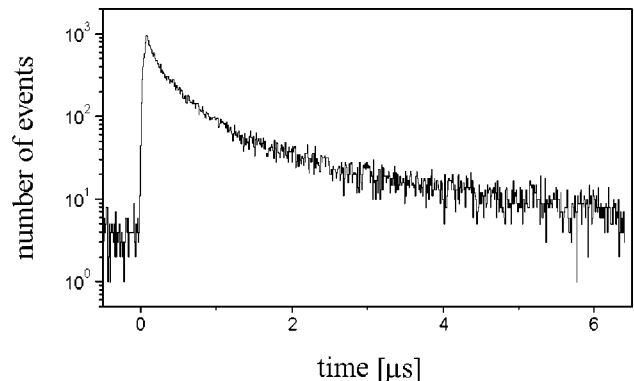
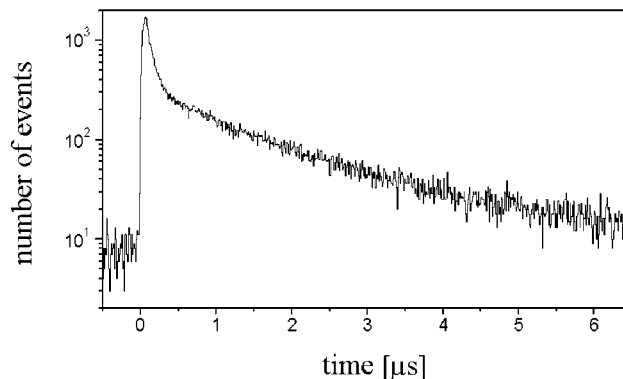
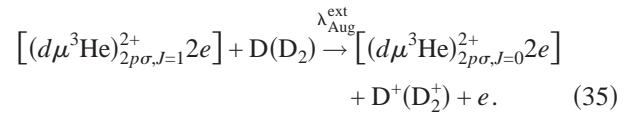
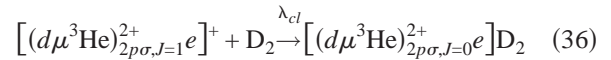


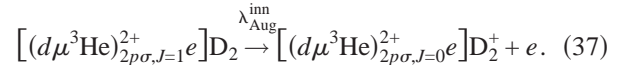
FIG. 8. Time distributions in runs III (left) and IV (right) within the energy range 5.74–7.50 keV.



In the second mechanism [34], the $J=1 \rightarrow J=0$ transition involves a number of molecular processes. However, the corresponding transition rate is essentially determined by a formation of molecular cluster



and a subsequent inner electron conversion



The first mechanism yields an effective $J=1 \rightarrow J=0$ transition rate

$$\tilde{\lambda}_{10} = \frac{\lambda_n \lambda_{\text{Aug}}^{\text{ext}} \varphi^2 c_{\text{D}} c_{\text{He}}}{\lambda_{\text{dec}}^1 + \lambda_{\text{Aug}}^{\text{ext}} \varphi c_{\text{D}} + \lambda_n \varphi c_{\text{He}}} \quad (38)$$

the second mechanism gives

$$\tilde{\lambda}_{10} = \frac{\lambda_{cl} \lambda_{\text{Aug}}^{\text{inn}} \varphi c_{\text{D}}}{\lambda_{\text{dec}}^1 + \lambda_{\text{Aug}}^{\text{inn}} + \lambda_{cl} \varphi c_{\text{D}}} \quad (39)$$

(see Refs. [43,44]). The effective $d\mu^3\text{He}$ decay rates for both rotational states, $J=0$ and $J=1$ are defined as

$$\lambda_{\text{dec}}^J = \lambda_{\gamma}^J + \lambda_e^J + \lambda_p^J. \quad (40)$$

TABLE VII. Experimental results for the muonic deuterium ground state disappearance rate and the $d\mu^3\text{He}$ molecular formation rate.

Runs	$\lambda_{d\mu}$ (μs^{-1})	$\lambda_{d^3\text{He}}$ (μs^{-1})
III	1.152(36) _{stat} (30) _{syst}	240(13) _{stat} (15) _{syst}
IV	2.496(58) _{stat} (100) _{syst}	244(6) _{stat} (16) _{syst}
Average		242(20)
Maev <i>et al.</i> [74]		232(9), 233(16) ^a
Gartner <i>et al.</i> [28]		185.6(77)

^aAt 50 and 39.5 K, respectively.

Because the effective transition rate $\tilde{\lambda}_{10}$ is model dependent, the ratio $\tilde{\lambda}_{10}/\lambda_{\text{dec}}^1$ may allow us to check the validity of both models. A proposal for a corresponding experiment was presented in Refs. [43,44]. It exploits the J dependence of the probability for the radiative $d\mu^3\text{He}$ decay ratio $\kappa_{d\mu\text{He}}$. An unequivocal identification of the $J=1 \rightarrow J=0$ transition mechanism should be possible by measuring the 6.85 keV γ -ray yields for a series of different densities of $\text{D}_2 + ^3\text{He}$ mixtures. The density dependence of $\kappa_{d\mu\text{He}}$ normalized to a single $d\mu^3\text{He}$ molecule is

$$\kappa_{d\mu\text{He}} = \frac{1}{\lambda_{\text{dec}}^1 + \tilde{\lambda}_{10}} \left[\lambda_{\gamma}^1 + \frac{\tilde{\lambda}_{10}\lambda_{\gamma}^0}{\lambda_{\text{dec}}^0} \right]. \quad (41)$$

Here, the decay rates $\lambda_{\text{dec}}^0 = 6 \times 10^{11} \text{ s}^{-1}$, $\lambda_{\gamma}^0 = 1.8 \times 10^{11} \text{ s}^{-1}$ [30], $\lambda_{\text{dec}}^1 = 7 \times 10^{11} \text{ s}^{-1}$, and $\lambda_{\gamma}^1 = 1.55 \times 10^{11} \text{ s}^{-1}$ (obtained by averaging the corresponding results taken from Refs. [27,29,30,75–80]) are model independent. Concerning the first mechanism, we used $\lambda_n = 2 \times 10^{13} \text{ s}^{-1}$, $\lambda_{\text{Aug}}^{\text{ext}} = 8.5 \times 10^{11} \text{ s}^{-1}$ [31], and $\lambda_{\text{Aug}}^{\text{ext}} = 10^{10} \text{ s}^{-1}$ [32,33]. For the second mechanism, we used $\lambda_{cl} = 3 \times 10^{13} \text{ s}^{-1}$ and $\lambda_{\text{Aug}}^{\text{inn}} = 10^{12} \text{ s}^{-1}$ [34]. All density dependent rates are normalized to LHD.

As can be seen from Fig. 9, our experimental values of $\kappa_{d\mu\text{He}}$ are in better agreement with the theoretical results corresponding to the first mechanism as described in Czaplinski *et al.* [31–33]. More refined calculations of the $J=1 \rightarrow J=0$

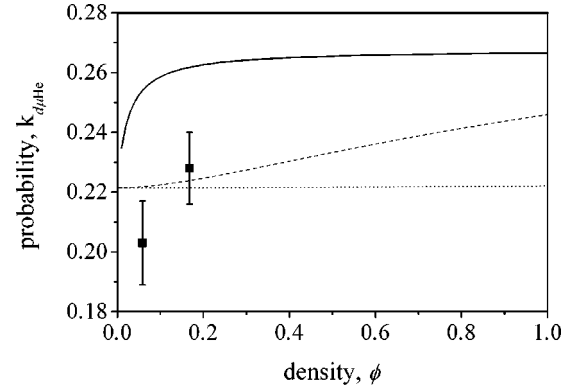


FIG. 9. Density dependence of the γ -decay branching ratio $\kappa_{d\mu\text{He}}$. Points with error bars are our experimental values. The solid line corresponds to the second mechanism with $\lambda_{\text{Aug}}^{\text{inn}} = 10^{12} \text{ s}^{-1}$ [34]. The dashed lines represents the first mechanism with $\lambda_{\text{Aug}}^{\text{ext}} = 8.5 \times 10^{11} \text{ s}^{-1}$ [31], whereas the dotted lines is given for $\lambda_{\text{Aug}}^{\text{ext}} = 10^{10} \text{ s}^{-1}$ [32,33].

transition including realistic $(\text{D}-d\mu^3\text{He})^{0,(+ \text{ or } 2+)}$ interaction potentials have, however, to be performed before definite conclusions can be drawn. Calculations in Refs. [32,33] go in this sense but within the framework of a semiclassical treatment. Such a treatment seems rather problematic considering the collision energies in such a system. More accurate, i.e., purely quantum mechanical calculations are now in progress.

D. Delayed K series transitions of μHe atoms

The relative intensities $I_{\text{del},x}$ and $I_{\text{del},x-e}$ of delayed μHe K series transitions were determined by measuring the $N_{\text{del},x}$ events during a time interval t_{γ} after the muon stop (see Table IX). The corresponding relative intensities were obtained from the ratios

$$I_{\text{del},x} = \frac{N_{\text{del},x}}{[\eta_x \varepsilon_{x\alpha}]} \bigg/ \sum_{x=\alpha,\beta,\gamma} \frac{N_{\text{del},x}}{[\eta_x \varepsilon_{x\alpha}]} \quad (42)$$

Our results should, in principle, coincide with the prompt intensities of K series transitions if we assume that the en-

TABLE VIII. Experimental results concerning formation and decay processes of $d\mu^3\text{He}$ molecules obtained from runs III and IV. “Full” stands for the full statistics, whereas del- e represents the delayed electron criterion. The 6.85 keV γ rays were measured within an energy range 5.74–7.55 keV. The time intervals for the γ rays and electrons are also given.

Parameter	Units	Run III		Run IV	
		full	del- e	full	del- e
t_{γ}	(μs)	[(-0.03)–(+2.5)]	[(-0.03)–(+2.5)]	[(-0.03)–(+1.8)]	[(-0.03)–(+1.8)]
$t_e - t_{\gamma}$	(μs)		(0.08–4.6)		(0.08–4.9)
$N_{6.85}$	(10^3)	17.42(21)	2.15(6)	20.07(23)	2.63(7)
$N_{\text{tot}}^{d\mu^3\text{He}}$	(10^3)	20.81(136)	20.86(136)	16.50(70)	16.41(72)
$N_{\gamma}^{d\mu^3\text{He}}$	(10^3)	4.20(10)	4.37(17)	3.76(10)	3.53(18)
$\varepsilon_{6.85}(1 - \eta_{6.85})$	(10^{-5})	4.15(8)	5.76(15)	6.26(19)	8.72(32)
$\kappa_{d\mu\text{He}}$		0.203(14)	0.209(17)	0.228(12)	0.213(15)

TABLE IX. Delayed relative muonic x-ray intensities for ${}^3\text{He}$ and ${}^4\text{He}$ atoms.

Run	Units	III (${}^3\text{He}$)	IV (${}^4\text{He}$)
t_γ	(μs)	(0.1–2.5)	(0.1–1.8)
$t_e - t_\gamma$	(μs)	(0.08–4.6)	(0.08–4.9)
$I_{\text{del},\alpha}$	(%)	0.605(75)	0.728(85)
$I_{\text{del},\beta}$	(%)	0.185(47)	0.160(48)
$I_{\text{del},\gamma}$	(%)	0.209(62)	0.112(60)

ergy distribution of the incoming muon as well as the primary μHe atom excited states distribution due to direct muon capture are the same as the corresponding ones for muons freed after the d - d fusion. The observed prompt relative intensities of the corresponding K series transitions (see Table III) are, however, different from the delayed ones indicating that the above conditions are probably not fulfilled.

V. CONCLUSIONS

The measured relative intensities of muonic K x rays in $\mu{}^3\text{He}$ and $\mu{}^4\text{He}$ atoms (see Tables III and V) agree well with other experiments. Regarding the q_{1s}^{He} probability for a $d\mu$ atom to reach its ground state in a $\text{D}_2 + {}^3\text{He}$ mixture at two different densities, our results are

$$q_{1s}^{\text{He}} = (0.882 \pm 0.018) \quad \varphi = 0.0585$$

and

$$q_{1s}^{\text{He}} = (0.844 \pm 0.020) \quad \varphi = 0.1680, \quad (43)$$

in agreement with theoretical calculations for an average $d\mu$ -He collision energy of around 8 eV.

As for the $d\mu{}^3\text{He}$ molecular formation rate $\lambda_d{}^3\text{He}$ for both our mixtures, our averaged value is

$$\lambda_d{}^3\text{He} = (242 \pm 20) \mu\text{s}^{-1}. \quad (44)$$

Our result agrees very well with the measurement of Maev *et al.* [74], but is in disagreement with the work of Gartner *et al.* [28]. This difference has not yet been understood.

Concerning the radiative decay branching ratio $\kappa_{d\mu\text{He}}$ for $d\mu{}^3\text{He}$, also measured for two different densities of the $\text{D}_2 + {}^3\text{He}$ mixture, the measured values

$$\kappa_{d\mu\text{He}} = (0.203 \pm 0.014) \quad \varphi = 0.0585$$

and

$$\kappa_{d\mu\text{He}} = (0.228 \pm 0.012) \quad \varphi = 0.1680 \quad (45)$$

are in agreement (within both error limits) for both densities, but disagree somewhat with the recent results by Augsburg *et al.* [20], $\kappa_{d\mu\text{He}} = (0.301 \pm 0.061)$, measured at an helium concentration approximately twice as big, namely, $c_{\text{He}} = 0.0913$.

Finally, the relative intensities of the delayed K series transitions $I_{\text{del},x}^{\text{D/He}}$ of μHe atoms, due to direct ${}^3\text{He}$ muon capture or due to muon transfer from deuterium to helium, after the muons were freed after d - d fusion, were also measured. They differ from the prompt relative intensities, probably due to a different primary distribution of excited states.

In conclusion, we were able to measure various interesting characteristics of muonic atom (MA) and muonic molecule (MM) processes occurring in pure helium and in $\text{D}_2 + {}^3\text{He}$ mixtures with good accuracy. This was possible by exploiting different germanium detectors for γ -ray detection in a wide energy range [3 keV–10 MeV], silicon $\text{Si}(dE - E)$ telescopes for the detection of charged particles coming from nuclear fusion or nuclear muon capture by ${}^3\text{He}$ and muon decay electron detectors. The self-consistent methods increased the reliability of the presented results. Further measurements of quantities such as the q_{1s}^{He} probability and the $\kappa_{d\mu\text{He}}$ branching ratio in a wider range of target densities and helium concentrations should significantly improve the accuracy of the corresponding values and clarify the complicated picture of muonic processes occurring in deuterium-helium targets.

ACKNOWLEDGMENTS

This work was supported by the Russian Foundation for Basic Research, Grant No. 01-02-16483, the Polish State Committee for Scientific Research, the Swiss National Science Foundation, and the Paul Scherrer Institute. The authors would like to thank Dr. R. Jacot-Guillarmod, Dr. C. Petitjean, A. Del Rosso, N. I. Zamiatin, and C. Donche-Gay for their help during the preparation of these experiments.

- [1] C. Petitjean, *Hyperfine Interact.* **138**, 191 (2001).
- [2] V. M. Bystritsky *et al.*, *Yad. Fiz.* **58**, 808 (1995) [*Phys. At. Nucl.* **58**, 746 (1995)].
- [3] V. M. Bystritsky, *Yad. Fiz.* **58**, 688 (1995) [*Phys. At. Nucl.* **58**, 631 (1995)].
- [4] G. M. Marshall *et al.*, *Hyperfine Interact.* **138**, 203 (2001).
- [5] K. Nagamine, *Hyperfine Interact.* **138**, 5 (2001).
- [6] C. Petitjean, *Nucl. Phys. A* **543**, 79c (1992).
- [7] G. A. Fesenko and G. Y. Korenman, *Hyperfine Interact.* **101/102**, 91 (1996).
- [8] M. P. Faifman and L. I. Men'shikov, *Hyperfine Interact.* **138**,

- 61 (2001).
- [9] J. S. Cohen, *RIKEN Rev.* **20**, 8 (1999).
- [10] V. E. Markushin and T. S. Jensen, *Hyperfine Interact.* **138**, 71 (2001).
- [11] A. Adamczak and M. P. Faifman, *Phys. Rev. A* **64**, 052705 (2001).
- [12] V. E. Markushin, *Phys. Rev. A* **50**, 1137 (1994).
- [13] V. M. Bystritsky *et al.*, *Phys. Rev. A* **53**, 4169 (1996).
- [14] T. S. Jensen and V. E. Markushin, *Hyperfine Interact.* **138**, 113 (2001).
- [15] V. P. Popov and V. N. Pomerantsev, *Hyperfine Interact.* **138**,

- 109 (2001).
- [16] V. M. Bystritsky *et al.*, *Eur. Phys. J. D* **8**, 75 (2000).
- [17] V. M. Bystritsky, W. Czapliński, and N. Popov, *Eur. Phys. J. D* **5**, 185 (1999).
- [18] A. V. Kravtsov and A. I. Mikhailov, *Phys. Rev. A* **49**, 3566 (1994).
- [19] S. Sakamoto, K. Ishida, T. Matsuzaki, and K. Nagamine, *Hyperfine Interact.* **119**, 115 (1999).
- [20] M. Augsburg *et al.*, *Phys. Rev. A* **68**, 022712 (2003).
- [21] F. Kottmann, in *Muonic Atoms and Molecules*, edited by L. A. Schaller and C. Petitjean (Birkhäuser Verlag, Basel, 1993), pp. 219–233.
- [22] S. Tresch *et al.*, *Phys. Rev. A* **58**, 3528 (1998).
- [23] B. Lauss *et al.*, *Phys. Rev. Lett.* **76**, 4693 (1996).
- [24] V. M. Bystritsky *et al.*, *Zh. Eksp. Teor. Fiz.* **84**, 1257 (1983) [*Sov. Phys. JETP* **57**, 728 (1983)].
- [25] Y. A. Aristov *et al.*, *Yad. Fiz.* **33**, 1066 (1981) [*Sov. J. Nucl. Phys.* **33**, 564 (1981)].
- [26] S. Tresch *et al.*, *Phys. Rev. A* **57**, 2496 (1998).
- [27] A. V. Kravtsov, A. I. Mikhailov, and V. I. Savichev, *Hyperfine Interact.* **82**, 205 (1993).
- [28] B. Gartner *et al.*, *Phys. Rev. A* **62**, 012501 (2000).
- [29] Y. Kino and M. Kamimura, *Hyperfine Interact.* **82**, 195 (1993).
- [30] W. Czapliński, A. Kravtsov, A. Mikhailov, and N. Popov, *Phys. Lett. A* **233**, 405 (1997).
- [31] W. Czapliński, M. Filipowicz, E. Guła, A. Kravtsov, A. Mikhailov, and N. Popov, *Z. Phys. D: At., Mol. Clusters* **37**, 283 (1996).
- [32] W. Czapliński, A. I. Mikhailov, and I. A. Mikhailov, *Hyperfine Interact.* **142**, 577 (2002).
- [33] W. Czapliński, E. Gula, and N. Popov, *Kerntechnik* **67**, 290 (2002).
- [34] L. N. Bogdanova, S. S. Gershtein, and L. I. Ponomarev, *Pis'ma Zh. Eksp. Teor. Fiz.* **67**, 89 (1998) [*JETP Lett.* **67**, 99 (1998)].
- [35] F. M. Pen'kov, *Yad. Fiz.* **60**, 1003 (1997) [*Phys. At. Nucl.* **60**, 897 (1997)].
- [36] V. F. Boreiko *et al.*, *Nucl. Instrum. Methods Phys. Res. A* **416**, 221 (1998).
- [37] P. E. Knowles *et al.*, *Hyperfine Interact.* **138**, 289 (2001).
- [38] V. M. Bystritsky *et al.*, *Phys. Rev. A* **69**, 012712 (2004).
- [39] E. M. Maev *et al.*, *Hyperfine Interact.* **118**, 171 (1999).
- [40] W. Czapliński, A. Kravtsov, A. Mikhailov, and N. Popov, *Phys. Lett. A* **219**, 86 (1996).
- [41] W. Czapliński, A. Kravtsov, A. Mikhailov, and N. Popov, *Eur. Phys. J. D* **3**, 223 (1998).
- [42] L. N. Bogdanova, V. I. Korobov, and L. I. Ponomarev, *Hyperfine Interact.* **118**, 183 (1999).
- [43] V. M. Bystritsky and F. M. Pen'kov, *Yad. Fiz.* **62**, 316 (1999) [*Phys. At. Nucl.* **62**, 281 (1999)].
- [44] V. M. Bystritsky, M. Filipowicz, and F. M. Pen'kov, *Nucl. Instrum. Methods Phys. Res. A* **432**, 188 (1999).
- [45] R. Schmidt *et al.*, *Eur. Phys. J. D* **3**, 119 (1998).
- [46] P. Hauser, F. Kottmann, C. Lüchinger, and R. Schaeren, in *Muonic Atoms and Molecules*, edited by L. A. Schaller and C. Petitjean (Birkhäuser Verlag, Basel, 1993), pp. 235–241.
- [47] A. Adamczak, *Hyperfine Interact.* **101/102**, 113 (1996).
- [48] F. Kottmann *et al.*, *Hyperfine Interact.* **119**, 3 (1999).
- [49] T. Koike, *Hyperfine Interact.* **138**, 95 (2001).
- [50] E. Storm and H. I. Israel, *Nucl. Data, Sect. A* **7**, 565 (1970).
- [51] J. H. Hubbell, *Int. J. Appl. Radiat. Isot.* **33**, 1269 (1982).
- [52] E. M. Maev *et al.*, *Hyperfine Interact.* **101/102**, 423 (1996).
- [53] A. C. Phillips, F. Roig, and J. Ros, *Nucl. Phys. A* **237**, 493 (1975).
- [54] T. Suzuki, D. F. Measday, and J. P. Roalsvig, *Phys. Rev. C* **35**, 2212 (1987).
- [55] J. S. Cohen, *Phys. Rev. A* **25**, 1791 (1982).
- [56] H. P. von Arb *et al.*, *Phys. Lett.* **136**, 232 (1984).
- [57] M. Eckhause *et al.*, *Phys. Rev. A* **33**, 1743 (1986).
- [58] J. Cohen and M. C. Struensee, *Phys. Rev. A* **38**, 53 (1988).
- [59] W. R. Johnson, *Phys. Rev. Lett.* **29**, 1123 (1972).
- [60] R. Bacher, *Z. Phys. A* **315**, 135 (1984).
- [61] J. S. Cohen, R. L. Martin, and W. R. Wadt, *Phys. Rev. A* **27**, 1821 (1983).
- [62] F. Kottmann, in *Second International Symposium on the Interaction of Muons and Pions with Matter* (JINR, Dubna, 1987), p. 268.
- [63] G. Y. Korenman, S. V. Leonova, and V. P. Popov, *Muon Catal. Fusion* **5/6**, 49 (1990/91).
- [64] M. Bubak and V. M. Bystritsky (unpublished).
- [65] V. I. Petrukhin and V. M. Suvorov, *Zh. Eksp. Teor. Fiz.* **70**, 1145 (1976).
- [66] V. Balin *et al.*, *Muon Catal. Fusion* **2**, 105 (1988).
- [67] V. M. Bystritsky *et al.*, *Kerntechnik* **58**, 185 (1993).
- [68] D. V. Balin *et al.*, *Phys. Lett.* **141B**, 173 (1984).
- [69] D. V. Balin *et al.*, *Pis'ma Zh. Eksp. Teor. Fiz.* **40**, 318 (1984) [*JETP Lett.* **40**, 1112 (1984)].
- [70] A. A. Vorobyov, *Muon Catal. Fusion* **2**, 17 (1988).
- [71] G. A. Rinker, *Phys. Rev. A* **14**, 18 (1976).
- [72] V. M. Bystritsky *et al.*, *Kerntechnik* **64**, 294 (1999).
- [73] V. M. Bystritsky, A. V. Kravtsov, and N. P. Popov, *Muon Catal. Fusion* **5/6**, 487 (1990/1991).
- [74] E. M. Maev *et al.*, *Hyperfine Interact.* **119**, 121 (1999).
- [75] V. B. Belyaev, O. I. Kartavtsev, V. I. Kochkin, and E. A. Kolganova, *Hyperfine Interact.* **101/102**, 359 (1996).
- [76] S. S. Gershtein and V. V. Gusev, *Hyperfine Interact.* **82**, 185 (1993).
- [77] V. B. Belyaev, O. I. Kartavtsev, V. I. Kochkin, and E. A. Kolganova, *Phys. Rev. A* **52**, 1765 (1995).
- [78] V. I. Korobov, V. S. Melezhik, and L. I. Ponomarev, *Hyperfine Interact.* **82**, 31 (1993).
- [79] V. Belyaev, O. Kartavtsev, V. Kochkin, and E. A. Kolganova, *Z. Phys. D: At., Mol. Clusters* **41**, 239 (1997).
- [80] K. Ishida *et al.*, *Hyperfine Interact.* **82**, 111 (1993).